Biophysical Chemistry 135 (2008) 84–94

Contents lists available at ScienceDirect

Biophysical Chemistry

journal homepage: http://www.elsevier.com/locate/biophyschem

Numerical simulation of the phase separation in binary lipid membrane under the effect of stationary shear flow

Xiao-Bo Chen, Li-Sha Niu *, Hui-Ji Shi

Key Laboratory of Failure Mechanics, Department of Engineering Mechanics, Tsinghua University, Beijing 100084, PR China

ARTICLE INFO

Article history:
Received 9 February 2008
Received in revised form 26 March 2008
Accepted 26 March 2008
Available online 8 April 2008

Keywords:
Phase separation
Binary lipid membrane
Stationary shear flow
Time evolution

ABSTRACT

A numerical simulation of the phase separation in binary lipid membrane under the effect of stationary shear flow is performed. We numerically solved the modified two-dimensional time-dependent Ginzburg–Landau (TDGL) equations with an external velocity term, employing the CDS (i.e., Cell Dynamical System) technique. In the present simulation, stationary shear flows with different shear rates are taken into account. The evolution process of the phase separation is illustrated macroscopically via the snapshot figures and simulated scattering patterns at several typical moments. For each case, the growth exponents of the characteristic domain sizes in both directions parallel and perpendicular to the flow are studied, and the domain area as well. Also, the behavior of the excess viscosity has been investigated, which is a peculiar rheological indicator of such a membrane system with domain structures.

1. Introduction

Biological cell is the carrier and the fundamental unit of life. Each living cell is enclosed by a plasma membrane called epicyte in bioscience. Actually, the epicyte separates the cell's internal contents from the external environment, dominating the cell's functions such as the transport of materials, the intermediation of metabolisms, and the responder to medicaments, etc. The constitution of the epicyte is a multi-component lipid bilayer with various types of macromolecules such as intercalated proteins and cholesterols [1]. But in classical simplified models, such a plasma membrane is reduced to a bilayer containing merely one species of lipid molecule [2]. During the last two decades, in order to much more precisely investigate the properties and functions of the epicyte, an increasing amount of attentions have been paid to the heterogeneity of multi-component lipid membranes [3–6]. One of the most important membrane heterogeneity is biologically called “raft”, which is enriched in cholesterol, saturated lipids such as sphingomyelin, glycosphingolipids, and certain membrane proteins [7,8]. Because of the important roles of the rafts in regulating cell functions, including signalling, endocytosis, apoptosis, protein organization and so on, the complex process of their formation has aroused extensive interests [9–12].

As a matter of fact, due to the limitation of existing research techniques, it seems impossible to make an investigation into this process with veritable epicyte. Because the composition of the membrane of living eukaryotic cells is extremely complex, consisting of up to 500 different lipid species and numerous large molecules such as proteins. And also, the membrane is structurally and dynamically coupled to the extra-cellular matrix and the cytoskeleton network [13]. Therefore, most of the experimental or theoretical studies have been based on approximately simplified membrane models, e.g. binary lipid membrane, ternary lipid membrane and so forth. The raft formation is dominantly driven by lipid–lipid interactions under appropriate conditions (for example when the temperature is lowered) [14]. It is reliable to explore this mechanism by means of binary lipid membrane systems. In binary or multi-component lipid membranes, the phase separation caused by the differences in physical properties of the compositions is recognized to be responsible for the formation of rafts in epicyte. Owing to various lipid membrane systems and diverse methods, large quantities of experiments have been carried out in order to examine the domain formation and its role in the process of membrane shape transformation and budding [15–20]. Simultaneously, theoretical forecasts and numerical simulations came into our sight one after another ceaselessly. Kumar and Rao introduced an off-lattice kinetic Monte Carlo technique for studying the dynamics of multi-component membranes in vesicle form [21]. Laradji and Kumar recently studied the domain coarsening in multi-component bilayer fluid vesicles with dissipative particle dynamics in the absence of spontaneous curvature

* Corresponding author. Tel.: +86 10 62772921; fax: +86 10 62781824.
E-mail address: niulsh@mail.tsinghua.edu.cn (L.-S. Niu).

0301-4622/$ – see front matter © 2008 Elsevier B.V. All rights reserved.
doi:10.1016/j.bpc.2008.03.007

[22]. Wallace et al. investigated phase separation in a model asymmetric membrane by also using the Monte Carlo method [23]. Wada investigated the dynamics of phase separation in two-component fluid membranes confined between parallel and rigid bounding plates utilizing the CDS approach [24]. Reigada et al. presented a simple kinetic model of a two-component deformable and reactive bilayer [25].

To obtain more credible results, influential effects that were usually ignored in previous studies are gradually getting into people's consideration, and the effect of external shear flow is just among those. Indeed, when lipids cluster into locally planar bilayer structures to form biological membranes, the surrounding must be an aqueous environment and will undoubtedly bring in shear flows. In addition, biological cells are mostly living in liquid environment and undergoing shear forces from various kinds of flows. Representatively, the membrane of the red blood cell (RBC) is easily deformed by shearing forces [26], which affects its physiological function of transporting oxygen [27] and determines the hydrodynamic properties of the whole blood [28]. It has also been demonstrated that shear stress can stimulate cell metabolism and increase the membrane fluidity of vascular endothelial cells [29,30]. Accordingly, in the present work we will focus on the phase-separation process in a binary lipid membrane subjected to a stationary shear flow. The kinetics is described by the modified time-dependent Ginzburg–Landau equation with an external velocity term. Shear flows from weak regime to strong regime are considered and compared.

In fact, for its potential technological importance, phase separation has been intensively studied both theoretically and experimentally in many systems, such as polymer blends, metallic alloys, binary liquid mixtures [31–33]. Most of the theoretical investigations have been based on the well known Cahn–Hilliard system [34–36], which is also the fundamental theory supporting our present work. In recent years, there has been much interest in the dynamics of phase separation in the presence of certain external driving fields [37–43]. Our present work has benefited a lot from these previous studies which have revealed many differences between such systems and systems in thermal equilibrium.

This paper is schematically organized as follows. In Section 2, the model is specified, including the total energy functional and governing equations, and such complex equations are then solved using a numerical method on basis of the CDS approach. In Section 3, we devote to the simulated results and interrelated discussions. Finally in Section 4 some conclusions will be drawn.

2. Total energy functional and governing equations

As is shown in Fig. 1, our model is described as a single idealized tow-component membrane consisting of two incompatible amphiphiles *A* and *B*. It is assumed that ϕ_A and ϕ_B are the local volume fraction of *A* and *B* components respectively, which will satisfy the following relationship $\phi_A+\phi_B=1$.

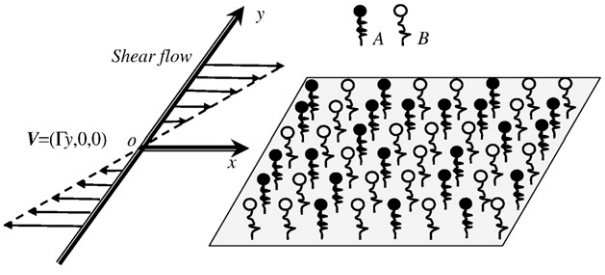

Fig. 1. Schematic view of a modulated lipid membrane composed of two amphiphiles *A* and *B* with an external stationary shear flow.

The membrane is defined as a two-dimensional plane surface with a concentration difference order parameter ϕ, where $\phi=\phi_A-\phi_B$. So as to satisfy the structural stability of the CDS method discussed in Ref. [44], instead of the classical potential proposed by Cahn and Hilliard, the mixing free energy caused by the interaction between the two components can be presented as

$$G_{\mathrm{mix}}=\int\int_{\Sigma}\left\{-\alpha\ \ln\ \ [\ \cosh\ \ (\phi)]+\frac{\beta}{2}\phi^2+\frac{D}{2}(\nabla\phi)^2\right\}\mathrm{d}x\mathrm{d}y \tag{1}$$

where the parameters α, β, D depend on the properties of the components and the temperature as well, Σ is the spatial field of the integration.

The deformable membrane surface is described by $[x,y,h(x,y)]$, where $h(x,y)$ is the off-plane displacement field for the local separation from the flat conformation. This representation is valid for surfaces that are nearly flat with only gradual variations of h. The rigidity of the membrane leads to an elastic bending energy contribution to the total energy [45], that is

$$\begin{aligned}G_{\mathrm{bending}}&=\frac{\kappa}{2}\int\int_{\Sigma}[2H-C_0(\phi)]^2\mathrm{d}A\\&=\frac{\kappa}{2}\int\int_{\Sigma}\left\{\left[\nabla^2h-C_0(\phi)\right]^2+\frac{1}{2}[C_0(\phi)]^2(\nabla h)^2\right\}\mathrm{d}x\mathrm{d}y\end{aligned} \tag{2}$$

where κ is the bending rigidity modulus, $C_0(\phi)$ is the spontaneous curvature, which reflects the shape asymmetry between the two components, usually simplified to be $C_0(\phi)=-\Lambda\phi$ (where Λ is called coupling constant). And H is the mean curvature with the expression as following

$$H=\frac{1}{2}\frac{\left(1+h_x^2\right)h_{yy}-2h_xh_yh_{xy}+\left(1+h_y^2\right)h_{xx}}{\left(1+h_x^2+h_y^2\right)^{3/2}} \tag{3}$$

where $h_{,x}=\partial h/\partial x$, $h_{,xy}=\partial h/(\partial x\partial y)$, etc. In our model, since $h_{,x}\ll 1$ and $h_{,y}\ll 1$, the approximation $H=\frac{1}{2}\frac{\nabla^2h}{\sqrt{1+|\nabla h|^2}}$ is allowed. And the area measure $\mathrm{d}A=\sqrt{1+(\nabla h)^2}\mathrm{d}x\mathrm{d}y$ is expanded to second order in h, which has given rise to the term $\frac{1}{2}[C_0(\phi)]^2(\nabla h)^2$.

The two-dimensional flat membrane can be assumed to be a small part of a large vesicle exactly. Therefore, surface tension has to be considered which suppresses membrane deviations from the flat state. Here comes another energy contribution [23], i.e. the frame energy

$$G_{\mathrm{frame}}=\int\int_{\Sigma}\frac{\lambda}{2}(\nabla h)^2\mathrm{d}x\mathrm{d}y \tag{4}$$

where λ is the surface tension.

With all the energy contributions analyzed above, the total energy functional of the modeled binary lipid membrane reads

$$F=G_{\mathrm{mix}}+G_{\mathrm{bending}}+G_{\mathrm{frame}}$$

$$\begin{aligned}F=\int\int_{\Sigma}\Bigg\{&\frac{\kappa}{2}\left(\nabla^2h+\Lambda\phi\right)^2+\left[\frac{\lambda}{2}+\frac{\kappa(\Lambda\phi)^2}{4}\right](\nabla h)^2-\alpha\ \ln\ \ [\ \cosh\ \ (\phi)]\\&+\frac{\beta}{2}\phi^2+\frac{D}{2}(\nabla\phi)^2\Bigg\}\mathrm{d}x\mathrm{d}y.\end{aligned} \tag{5}$$

For simplicity, we consider the case when the binary lipid membrane is subject to a stationary shear flow with a zero-divergence (i.e. $\nabla\cdot\boldsymbol{V}=0$) velocity field, which is given as $\boldsymbol{V}=(\Gamma y,0,0)$, where Γ is the spatially homogeneous shear rate.

In order to avoid complex work of analyzing dimensions, dimensionless parameters are firstly introduced to simplify all the notations mentioned in the foregoing paragraphs:

$$\begin{aligned} f &= F/k_BT,\ \tau = t/t_0,\ \gamma = \Gamma t_0, \tilde{\kappa} = \kappa/k_BT, \tilde{x} = x/a_0, \tilde{y} = y/a_0, \tilde{\lambda} \\ &= \lambda a_0^2/k_BT, \tilde{\Lambda} = \Lambda a_0, \tilde{\alpha} = \alpha a_0^2/k_BT, \tilde{\beta} = \beta a_0^2/k_BT, \tilde{D} = D/k_BT, \tilde{h} \\ &= h/a_0, \tilde{\mathbf{V}} = Vt_0/a_0 = (\gamma\tilde{y}, 0, 0). \end{aligned}$$

Thus Eq. (5) becomes

$$\begin{aligned} f = \int\int_{\tilde{\Sigma}} \Bigg\{ & \frac{\tilde{\kappa}}{2}\left(\nabla^2\tilde{h} + \tilde{\Lambda}\phi\right)^2 + \left[\frac{\tilde{\lambda}}{2} + \frac{\tilde{\kappa}\left(\tilde{\Lambda}\phi\right)^2}{4}\right] \\ & \times (\nabla\tilde{h})^2 - \tilde{\alpha}\ \ln\ [\cosh\ (\phi)] \\ & + \frac{\tilde{\beta}}{2}\phi^2 + \frac{\tilde{D}}{2}(\nabla\phi)^2 \Bigg\} d\tilde{x}d\tilde{y} \end{aligned} \tag{6}$$

here, k_B is the Boltzmann constant, T is the temperature of the system, a_0 and t_0 are the units of length and time scales, respectively. ∇ and ∇^2 are the gradient operator and Laplacian operator in the dimensionless unit plane.

The time evolution of the order parameter ϕ and that of the off-plane displacement $\tilde{h}$, are described by the convection–diffusion equations, which add external velocity terms to the two-dimensional time-dependent Ginzburg–Landau (TDGL) equations [46,47]

$$\frac{\partial\phi}{\partial\tau} + \nabla\cdot\left(\phi\,\tilde{\boldsymbol{V}}\right) = M\nabla^2\left(\frac{\delta f}{\delta\phi}\right) \Rightarrow \frac{\partial\phi}{\partial\tau} = -\,\tilde{\boldsymbol{V}}\cdot\nabla\phi + M\nabla^2\left(\frac{\delta f}{\delta\phi}\right) \tag{7A}$$

$$\frac{\partial\tilde{h}}{\partial\tau} + \nabla\cdot\left(\tilde{h}\tilde{\boldsymbol{V}}\right) = -N\left(\frac{\delta f}{\delta\tilde{h}}\right) \Rightarrow \frac{\partial\tilde{h}}{\partial\tau} = -\,\tilde{\boldsymbol{V}}\cdot\nabla\tilde{h} - N\left(\frac{\delta f}{\delta\tilde{h}}\right) \tag{7B}$$

where M and N are the phenomenological lateral mobility parameters. Then ignoring the terms behaving small quantities $(1/2M\tilde{\kappa}\tilde{\Lambda}\phi\left(\nabla\tilde{h}\right)^2$ in Eq. (8A), $1/2N\tilde{\kappa}\tilde{\Lambda}^2\left[\phi^2\nabla^2\tilde{h} + (\nabla\phi)\cdot\left(\nabla\tilde{h}\right)\right]$ in Eq. (8B), we obtain the governing equations for the phase-separation process

$$\frac{\partial\phi}{\partial\tau} = -\gamma\cdot\tilde{y}\frac{\partial\phi}{\partial\tilde{x}} + M\nabla^2\left[\left(\tilde{\kappa}\tilde{\Lambda}^2 + \tilde{\beta}\right)\phi - \tilde{\alpha}\ \tanh\ (\phi) - \tilde{D}\nabla^2\phi + \tilde{\kappa}\,\tilde{\Lambda}\nabla^2\tilde{h}\right] \tag{8A}$$

$$\frac{\partial\tilde{h}}{\partial\tau} = -\gamma\cdot\tilde{y}\frac{\partial\tilde{h}}{\partial\tilde{x}} - N\left[\tilde{\kappa}\nabla^2\nabla^2\tilde{h} + \tilde{\kappa}\tilde{\Lambda}\nabla^2\phi - \tilde{\lambda}\nabla^2\tilde{h}\right]. \tag{8B}$$

Noting that the highly non-linear governing equations are coupling the temporal field with the spatial field and the two parameters ϕ and $\tilde{h}$ are also coupled, numerical methods should be the only choice to solve such equations. With the temporal field discretized, and employing the Cell Dynamical System (CDS) approach proposed by Puri and Oono [44], the discrete governing equations are finally expressed as (refer to Appendix A for details)

$$\begin{aligned} \phi(n_x, n_y, \tau + \Delta\tau) = {} & \phi(n_x, n_y, \tau) + \Delta\tau \\ & \times\Bigg\{-\gamma\cdot\frac{1}{2}\tilde{y}[\phi(n_x+1, n_y, \tau) - \phi(n_x-1, n_y, \tau)] \\ & + M\nabla^2 I_\phi(n_x, n_y, \tau)\Bigg\} \end{aligned} \tag{9A}$$

$$\begin{aligned} \tilde{h}(n_x, n_y, \tau + \Delta\tau) = {} & \tilde{h}(n_x, n_y, \tau) + \Delta\tau \\ & \times\Bigg\{-\gamma\cdot\frac{1}{2}\tilde{y}\left[\tilde{h}(n_x+1, n_y, \tau) - \tilde{h}(n_x-1, n_y, \tau)\right] \\ & - N\nabla^2 I_{\tilde{h}}(n_x, n_y, \tau)\Bigg\} \end{aligned} \tag{9B}$$

where $I_\phi(\boldsymbol{n},\tau)$ and $I_{\tilde{h}}(\boldsymbol{n},\tau)$ are the discrete thermodynamic forces given by

$$\begin{aligned} I_\phi(\boldsymbol{n}, \tau) = {} & \left(\tilde{\kappa}\tilde{\Lambda}^2 + \tilde{\beta}\right)\phi(\boldsymbol{n}, \tau) - \tilde{\alpha}\ \tanh\ [\phi(\boldsymbol{n}, \tau)] - \tilde{D}\nabla^2\phi(\boldsymbol{n}, \tau) \\ & + \tilde{\kappa}\tilde{\Lambda}\nabla^2\tilde{h}(\boldsymbol{n}, \tau) \end{aligned} \tag{10A}$$

$$I_{\tilde{h}}(\boldsymbol{n}, \tau) = \tilde{\kappa}\nabla^2\tilde{h}(\boldsymbol{n}, \tau) + \tilde{\kappa}\tilde{\Lambda}\phi(\boldsymbol{n}, \tau) - \tilde{\lambda}\tilde{h}(\boldsymbol{n}, \tau). \tag{10B}$$

3. Results and discussions

In the present work, all the simulations have fixed the standard parameters to be $\tilde{\alpha}=1.3$, $\tilde{\beta}=1$, $\tilde{D}=0.5$, $\tilde{\kappa}=10/3$, $\tilde{\Lambda}=0.2$, $\tilde{\lambda}=0.01$, and $M=N=0.05$ [24]. As the interface width ξ between two domains is given by $\xi = \sqrt{\tilde{D}/(\tilde{\alpha}-1)}$, for the current set of parameters, we have $\xi=1.29$. The dimensionless time step is set to be $\Delta\tau=0.5$, and the shear rate has been changed as $\gamma = 0, 2\times10^{-5}, 4\times10^{-5}, 7\times10^{-5}, 1\times10^{-4}, 2\times10^{-4}, 3\times10^{-4}, 5\times10^{-4}$. The initial distribution of ϕ is specified by random numbers uniformly distributed in the range [−0.01,0.01] around the average value $\phi_0=0$, which corresponds to a completely disordered uniform state. Simultaneously the initial membrane shape is assumed to be perfectly flat which indicates $h(\boldsymbol{n},0)=0$. The variations of the height field are especially monitored and the condition $\langle\nabla\tilde{h}\rangle<0.05$ is successfully satisfied, so that the model has a real physical correspondence.

3.1. Linear stability analysis of the membrane system

In the absence of external shear flow, the stationary uniform state of the membrane system corresponds to $\phi=\phi_0$ and arbitrary $\tilde{h}_0$. The linear stability of the uniform solutions can be tested by adding small plane-wave perturbations with wave number k. A Fourier expansion is introduced as

$$\phi = \phi_0 + \sum_k \Phi_{k\tau} e^{ik\cdot r} \tag{11A}$$

$$\tilde{h} = \tilde{h}_0 + \sum_k H_{k\tau} e^{ik\cdot r} \tag{11B}$$

where $\phi_0=0$ and $\tilde{h}_0=0$ are the constant composition and height respectively. In the $k\neq0$ modes, Eqs. (8A) and (8B) become

$$\frac{\partial\Phi_{k\tau}}{\partial\tau} = -Mk^2\left[\left(f_0'' + \tilde{\kappa}\tilde{\Lambda}^2 + \tilde{D}k^2\right)\Phi_{k\tau} - \tilde{\kappa}\tilde{\Lambda}k^2 H_{k\tau}\right] \tag{12A}$$

$$\frac{\partial H_{k\tau}}{\partial\tau} = -N\left[-\tilde{\kappa}\tilde{\Lambda}k^2\Phi_{k\tau} + \left(\tilde{\kappa}k^4 + \tilde{\lambda}k^2\right)H_{k\tau}\right] \tag{12B}$$

where $f_0'' = \frac{\partial^2 f_0}{\partial\phi^2}|_{\phi=\phi_0} = -\tilde{\alpha}\left(1 - \tanh^2(\phi_0)\right) + \tilde{\beta}$ [23], $f_0(\phi)$is the two anterior terms in Eq. (1). Then, Eqs. (12A) and (12B) can be written as

$$\begin{bmatrix} \dot{\Phi}_{k\tau} \\ \dot{H}_{k\tau} \end{bmatrix} = \mathbb{R}\begin{bmatrix} \Phi_{k\tau} \\ H_{k\tau} \end{bmatrix} \tag{13}$$

where

$$\mathbb{R} = \begin{pmatrix} -Mk^2\left(\tilde{\kappa}\tilde{\Lambda}^2 + \tilde{\beta} - \tilde{\alpha}\left(1 - \tanh^2(\phi_0)\right) + \tilde{D}k^2\right) & M\tilde{\kappa}\tilde{\Lambda}k^4 \\ N\tilde{\kappa}\tilde{\Lambda}k^2 & -N\left(\tilde{\kappa}k^4 + \tilde{\lambda}k^2\right) \end{pmatrix}. \tag{14}$$

We assume that the solution of Eq. (13) has the following form

$$\Phi_{k\tau} = \Phi_{kw} e^{\omega_k \tau},\ H_{k\tau} = H_{kw} e^{\omega_k \tau}. \tag{15}$$

Substituting Eq. (15) into Eq. (13) we have

$$\omega_k \begin{bmatrix} \Phi_{k\tau} \\ H_{k\tau} \end{bmatrix} = \mathbb{R} \begin{bmatrix} \Phi_{k\tau} \\ H_{k\tau} \end{bmatrix}. \tag{16}$$

Hence the eigenvalue ω_k of the Jacobian associated with the matrix $\mathbb{R}$ corresponds to the linear growth rates of the perturbations. Solving the eigenvalue problem, we finally get

$$\omega_k = \frac{(\mathbb{R}_{11} + \mathbb{R}_{22}) \pm \sqrt{(\mathbb{R}_{11} - \mathbb{R}_{22})^2 + 4\mathbb{R}_{12}\mathbb{R}_{21}}}{2} \tag{17}$$

where $\mathbb{R}_{ij}(i,j = 1,2)$ are the components of the matrix $\mathbb{R}$.

Fig. 2 shows the growth rate ω_{*k} as a function of k for different coupling constant $\tilde{\Lambda}$ and surface tension $\tilde{\lambda}$. Other dimensionless parameters are set to the standard values (specified in the first paragraph of this section). The parameter $\omega_0 = Ma^2/4\tilde{D}$ is the maximal growth rate of a bulk spinodal decomposition [24], and $a = 1 - A = -0.3$ is the first parameter in the classical Ginzburg–Landau free energy [48]. A homogeneous distribution of $\phi(\phi_0 = 0)$ becomes unstable against perturbations with finite wave numbers. According to Fig. 2,

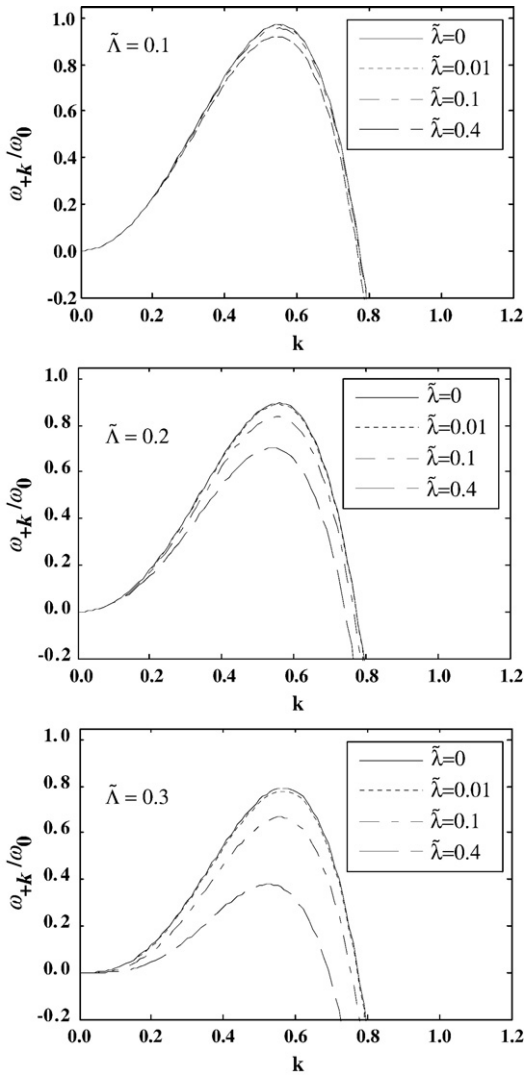

Fig. 2. Plots of ω_{*k} as a function of k for different values of $\tilde{\Lambda}$ and $\tilde{\lambda}$.

increasing $\tilde{\lambda}$ will reduce the range of unstable modes progressively, and increasing $\tilde{\Lambda}$ reduces the growth rate of perturbations and makes the influence of $\tilde{\lambda}$ more distinct.

3.2. Time evolution of phase morphologies

In this subsection, we present the results of the numerical integration of the governing equations, which enable us to follow the whole time history of the phase-separation process. In Fig. 3, the four snapshot pictures in the front of each row visibly show the time evolution of the phase morphologies, where regions with a positive order parameter (*A* rich phase; say, *A*-rich) are marked brightness while those with a negative order parameter (*B* rich phase; say, *B*-rich) are purely black. And the final image in each row is the membrane shape at the end moment of the present simulation.

When $\gamma = 0$, i.e. there is no shear flow applied to the membrane system, the system is quenched from a disordered phase state into a two-phase regime, mainly by force of the thermodynamic potential. In our model, since *A* and *B* are in equal concentrations initially, an isotropic bicontinuous structure emerges in the late stage of the phase-separation process. When shear flow is applied, the most obvious effect of shear flow on the phase morphology is that the growing domains are elongating in the direction of the flow, leading to an anisotropic morphology, just in agreement with the result of previous relevant studies [41,49]. More exactly, at the early stage while $\gamma\tau \leq 1$, the shear flow does not exhibit very conspicuous influence on the phase-separation process. And then, as the evolution time continues, the domains begin to have an anisotropic feature: the average direction of the domains becomes apparent and a string-like phase of domains can be observed. Along with the increasing strain, the elongating direction rotates and becomes more and more oriented parallel to the flow. The higher the shear rate is, the clearer the anisotropy will be. It is noted that for strong-shear regime, there is a stage at which domains break up just before stretching in the flow direction, as is clearly shown at $\tau = 50000$ for $\gamma = 3 \times 10^{-4}$. The domains are continuously stretching and breaking up until string-like domains are completely aligned with the flow direction. Subsequently, the shear flow only will act to make the domains more smooth. Typically, in the case of $\gamma = 5 \times 10^{-4}$, the shear rate is strong enough so that at $\tau = 100{,}000$ the string-like domains can be observed to extend macroscopically in the direction of the flow, forming an extremely anisotropic phase morphology. For the reason that the field $\tilde{h}$ displays a same evolution law as the field ϕ does [24], from this section on, our discussions will only focus on the field ϕ.

3.3. Dynamical evolution of the structure factor

For a more quantitative discussion about the kinetic ordering process, here we first consider the discrete Fourier transform of $\phi(\boldsymbol{n},\tau)$, which is defined as

$$\phi_{\boldsymbol{q}}(\tau) = \sum_{\boldsymbol{n}} \phi(\boldsymbol{n},\tau) \quad \exp \quad (i\boldsymbol{q} \cdot \boldsymbol{n}) \tag{18}$$

with the wave number $\boldsymbol{q} = 2\pi\boldsymbol{n}/L$ and $\boldsymbol{n} \in \{0,1,\ldots, L-1\}^2$. The main observable parameter for the description of the phase-separation kinetics is the structure factor $C(\boldsymbol{q},\tau)$, as is given by $C(\boldsymbol{q},\tau) = \langle \phi_{\boldsymbol{q}}(\tau)\phi_{-\boldsymbol{q}}(\tau) \rangle$, where the average is over the ensemble of the system. Actually, the structure factor is the direct result of scattering experiments, being a normal mode for phase separation at different locations.

As is presented in Fig. 4, when $\gamma = 0$, the structure factor is isotropic through the whole evolution process. It is clear that the scattering circular ring becomes smaller with increasing time, which means that the maximum of the scattering intensity shifts to smaller wave

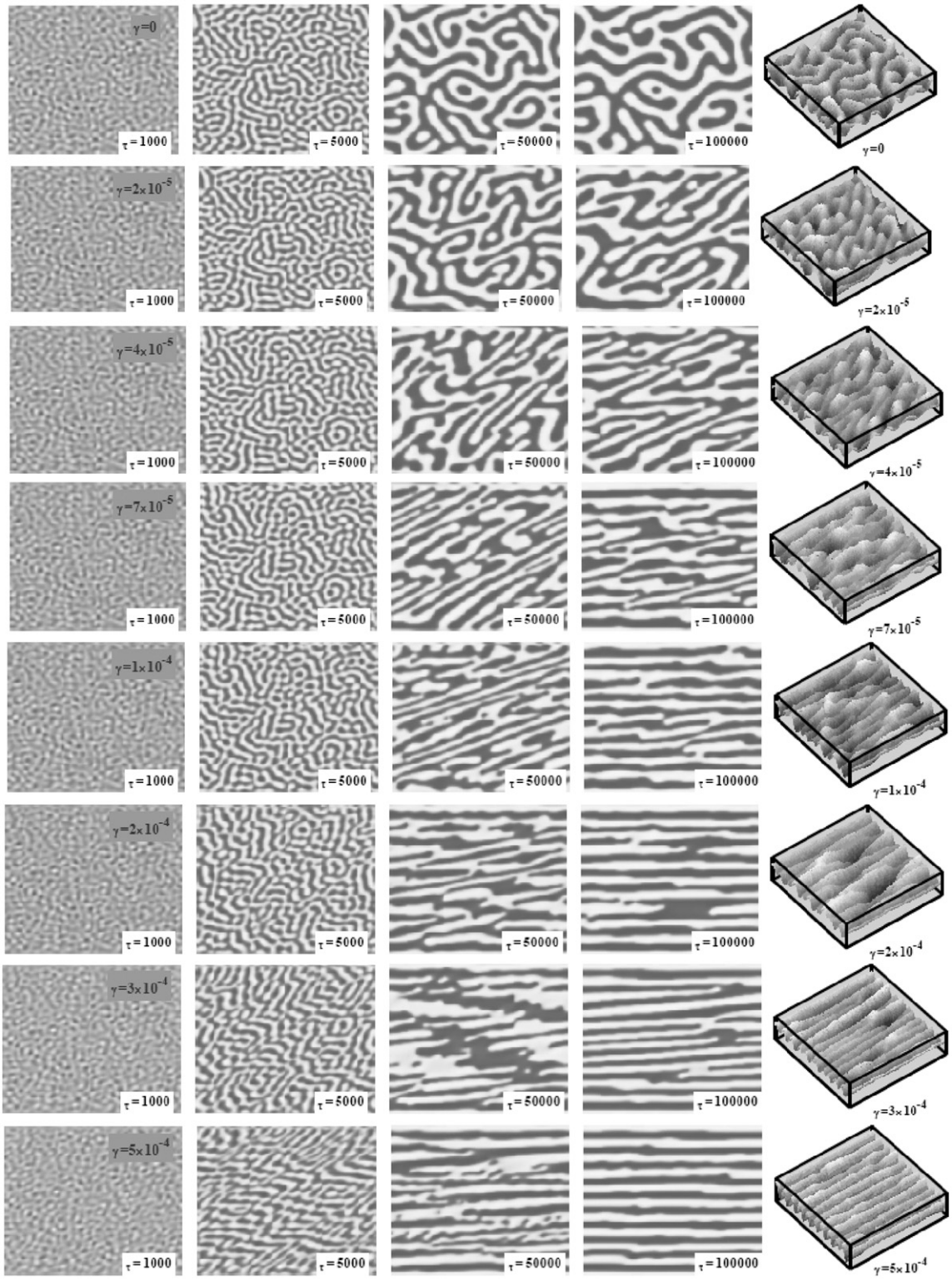

Fig. 3. Snapshot figures of the phase morphologies at $\tau = 1000$, 5000, 50,000, 100,000 and the membrane shape at $\tau = 100{,}000$ for each case of γ.

number. Then, when the shear flow is imposed, at the early stage, domains are formed but the shear flow has not produced sensible effects yet, as is discussed in the previous subsection. Thus, for each shear rate, the structure factor displays the typical isotropic circular ring and exhibits peaks at a finite wave number. This is corresponding to the early-time regime without sharp interfaces, as what happens in the case of no shear. But in later stage, shear-induced anisotropy becomes apparent, the scattering patterns collapse and rotate gradually to the y direction which is perpendicular to the flow direction, as has been experimentally observed in a similar phase-separating system [49]. When the shear rate is strong enough, at adequately late time the scattering pattern even transforms to two small dots located on the y axis, which will become almost invisible if complete string-like domains are shaped up and smoothed. Such

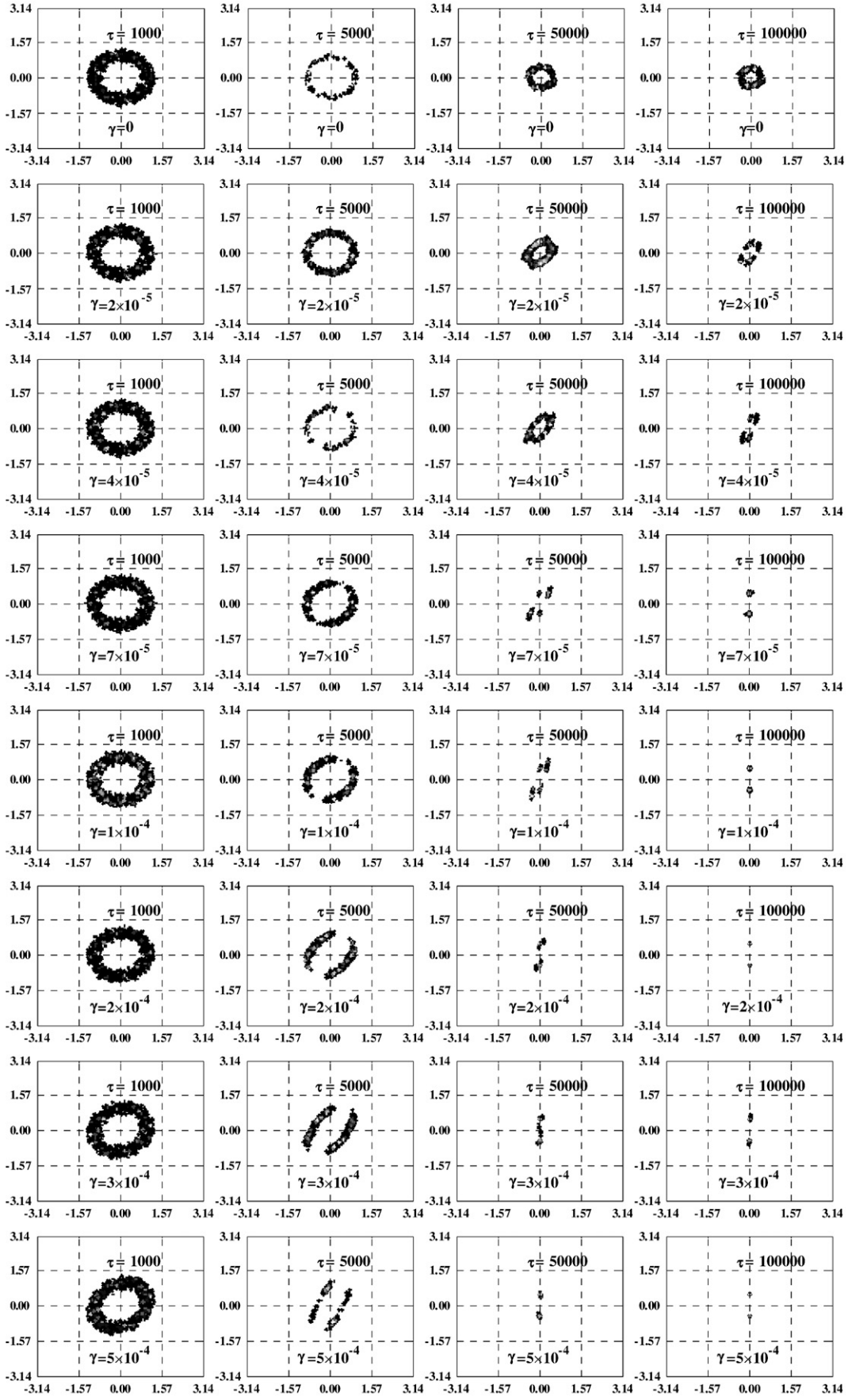

Fig. 4. Plots of $C(\boldsymbol{q},\tau)$ in the $\boldsymbol{q}(q_y-q_x)$ space at different moments for each case of γ.

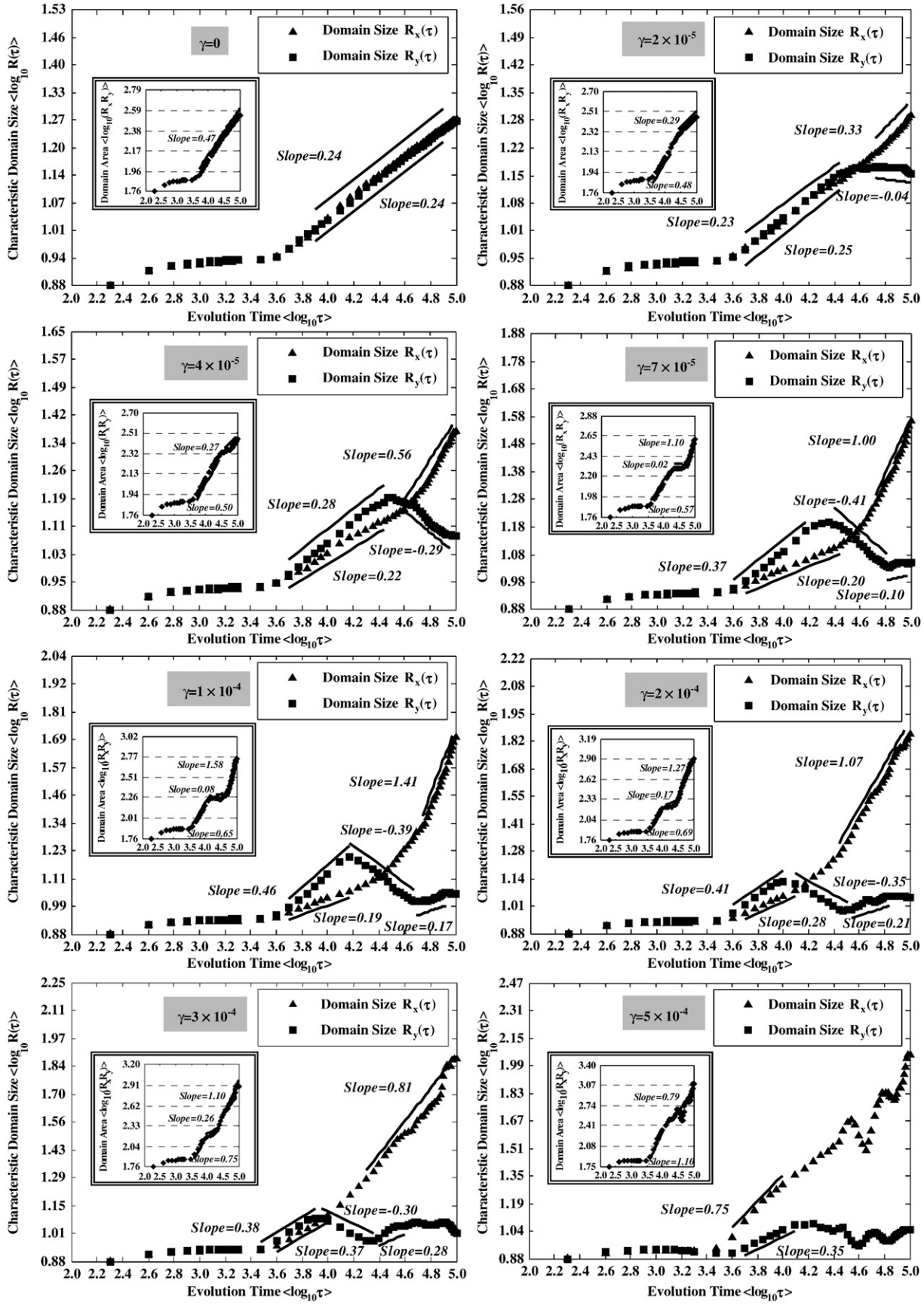

Fig. 5. Plots of time evolution of the characteristic domain sizes for each case of γ and the inset is the corresponding characteristic domain areas versus time, with each coordinate converted to logarithm.

anisotropic phenomenon reflects the domain elongation and rotation in the direction parallel to the flow and indicates a systematic existence of two characteristic scales in the size distribution of domains as will be discussed in the next subsection.

3.4. Time growth of characteristic domain sizes

From the knowledge of the structure factor $C(\boldsymbol{q},\tau)$, we are allowed to compute the characteristic domain sizes in the direction parallel to the flow and that perpendicular to it with the following formulas

$$R_x(\tau)=\frac{2\pi}{\sqrt{\langle q_x^2(\tau)\rangle}}, R_y(\tau)=\frac{2\pi}{\sqrt{\langle q_y^2(\tau)\rangle}} \tag{19}$$

where

$$\langle q_x^2(\tau)\rangle=\frac{\int q_x^2 C(\boldsymbol{q},\tau)\mathrm{d}\boldsymbol{q}}{\int C(\boldsymbol{q},\tau)\mathrm{d}\boldsymbol{q}}, \langle q_y^2(\tau)\rangle=\frac{\int q_y^2 C(\boldsymbol{q},\tau)\mathrm{d}\boldsymbol{q}}{\int C(\boldsymbol{q},\tau)\mathrm{d}\boldsymbol{q}}. \tag{20}$$

According to Fig. 5, there is a critical time point $\tau_c\approx 3000$ in the early stage of all such phase-separation events, before which we have an early-time isotropic evolution. Ordered domains of the equilibrium phases are forming at a very gentle speed. In absence of shear flow, the thermodynamics driving diffusion is dominating the whole segregation process, coinciding with the results and inferences presented in previous subsections. The growth exponents of the two characteristic domain sizes stay equal, namely $R_x(\tau)\sim\tau^{0.24}$ and $R_y(\tau)\sim\tau^{0.24}$. It should be noted that in two-dimensional systems diffusive Lifshitz–Slyozov theory gives the growth law $R(\tau)\sim\tau^{1/3}$. Here in our model, the phase separation is accompanied by the change of the membrane shape. During this process, some energy of the whole system has been stored as curvature energy, leading to a slower phase evolution law. Just as has been reported in other studies, curvature considerably slows down the coarsening segregation process [25]. When the shear flow is applied, the shear-induced anisotropy becomes more and more pronounced, the growth exponents of $R_x(\tau)$ and $R_y(\tau)$ start to differ from each other at an early or later moment. As is shown Fig. 5 and Table 1, in the cases of neither too weak nor too strong shear rate, after the critical time $\tau_c\approx 3000$, for $R_x(\tau)\sim\tau^{\alpha_x}$, prominently the exponent α_x has two different values, while in the relationship $R_y(\tau)\sim\tau^{\alpha_y}$, α_y has three step values. And it is found that for the cases of $0<\gamma\leq 3\times10^{-4}$, $R_y(\tau)$ reaches a maximum at the inflexion between the first step and the second step. In fact, this inflexion corresponds to the time when the domains have elongated along the y axis at utmost. As the shear rate is increased, such an inflexion will appear at an earlier moment.

Such phenomena can be interpreted as follows: After the critical time $\tau_c\approx 3000$, the strain exerted by the flow can produce mainly two different effects, in particular the breakup and recombination of domains. Whether the exponents are positive or negative is just determined by the competition between the two combative effects. Actually, the fragmentation process is accompanied by the formation of isotropic clusters, which grow by the force of diffusion. Then the clusters join to each other as a result of the effect from the flow. From our results, when the shear rate is quite weak, saying $\gamma=2\times10^{-5}$ and $\gamma=4\times10^{-5}$, it seems impossible for α_y to display the third step value. Whereas when the shear rate is strong enough to be $\gamma=5\times10^{-4}$, the first two step values of α_y have gone out of our sight as well as the first value of α_x. Furthermore, at the long time later stage, the domains stretch and break up cyclically, producing an oscillatory pattern around the typical size. It can be found that there is also a maximum value of $R_y(\tau)$, but it comes about in a dissimilar way compared to that for $0<\gamma\leq 3\times10^{-4}$.

Subsequently, in order to better understand the effect of shear flow on the power law of the domain growth, the exponents of different steps in the relationships $R_x(\tau)\sim\tau^{\alpha_x}$, $R_y(\tau)\sim\tau^{\alpha_y}$ and $C_A(\tau)\sim\tau^S$ are exhibited in Table 1, where we define $C_A(\tau)=R_x(\tau)R_y(\tau)$ as the characteristic domain area. It is quite clear that along with the accretion of shear rate, disciplines of increasing or decreasing have acted on these slope values. From these results, we interestingly find that most of such values reach their extremum when the shear rate is around 7×10^{-5} or 1×10^{-4}, while S_1 keeps getting lager as γ increases.

Table 1
The growth exponents of the characteristic domain sizes and domain area, α_{xi}, α_{yi}, S_i are the corresponding step values

γ		0	2×10^{-5}	4×10^{-5}	7×10^{-5}	1×10^{-4}	2×10^{-4}	3×10^{-4}	5×10^{-4}
R_x	α_{x1}	0.24	0.23	0.22	0.20	0.19	0.28	0.37	-
	α_{x2}	0.24	0.33	0.56	1.00	1.41	1.07	0.81	0.75
R_y	α_{y1}	0.24	0.25	0.28	0.37	0.46	0.41	0.38	-
	α_{y2}	0.24	−0.04	−0.29	−0.41	−0.39	−0.35	−0.30	-
	α_{y3}	0.24	-	-	0.10	0.17	0.21	0.28	0.35
C_A	S_1	0.47	0.48	0.50	0.57	0.65	0.69	0.75	1.10
	S_2	0.47	0.29	0.27	0.02	0.08	0.17	0.26	-
	S_3	0.47	-	-	1.10	1.58	1.27	1.10	0.79

3.5. Behavior of the excess viscosity

The viscosity of a biological membrane is an important factor in determining the rate at which the membrane can undergo deformation on a macroscopic scale, and it also influences the rate at which particles can diffuse in the plane of the surface. These processes play important roles in a wide variety of biological phenomena [50]. Changes in viscosity of the erythrocyte plasma membrane were found in patients with diabetes mellitus, which would cause the decrease in oxygen binding and increase in deoxyhemoglobin concentration during diabetes mellitus [51]. Due to the domain interface during the phase separation, the membrane system macroscopically shows up excess stresses as its viscoelastic response. Originally arising from the excess shear stress σ_{xy}^{e}, the excess viscosity η_e can be expressed as $\eta_e=\eta_{\mathrm{mix}}-\eta_{\mathrm{one}}$, where η_{mix} is the measured effective viscosity of the membrane with domain microstructures and η_{one} is the background viscosity of the mixture in a homogenized state without domains [42]. Here σ_{xy}^{e} and η_e are introduced as [52]

$$\sigma_{xy}^{e}(\tau)=\int_{|\boldsymbol{q}|\leq q_c}\frac{1}{(2\pi)^d}q_x q_y C(\boldsymbol{q},\tau)\mathrm{d}\boldsymbol{q} \tag{21}$$

$$\eta_e(\tau)=\frac{\sigma_{xy}^{e}}{\gamma}=\frac{1}{\gamma}\int_{|\boldsymbol{q}|\leq q_c}\frac{1}{(2\pi)^d}q_x q_y C(\boldsymbol{q},\tau)\mathrm{d}\boldsymbol{q} \tag{22}$$

where q_c is a phenomenological cutoff, d is the spatial dimension and equals to 2 in our model.

According to Fig. 6, for $\gamma=0$, we cannot define a η_e, but the excess shear stress σ_{xy}^{e} still comes about and appears to be at a fixed value after an initial rise. Then for $\gamma\neq0$, the quantity η_e characterizes the domain contribution, and the membrane can exhibit strong non-Newtonian character when the domains are strongly deformed by the shear flow. Starting from zero in correspondence with the isotropic initial condition, η_e grows up with time to reach a global-maximum and later decays, in accord with the experimental result of Miyazawa et al. [53]. The relative maximum of η_e corresponds to the time when $R_y(\tau)$ reaches its maximum. At that moment, the domains are maximally stretching along the direction perpendicular to the flow, as the discussions in the previous subsections. Apparently, its position on the time axis moves leftwards as the shear rate is increased within the range $0<\gamma\leq 3\times10^{-4}$. However, for $\gamma=4\times10^{-4}$ and $\gamma=5\times10^{-4}$, such a law will not go into operation, for the sake of the dissimilarity mentioned in Section 3.4.

In fact, in the early stage, the system is quenched from the disordered phase to a more and more ordered state, causing the excess

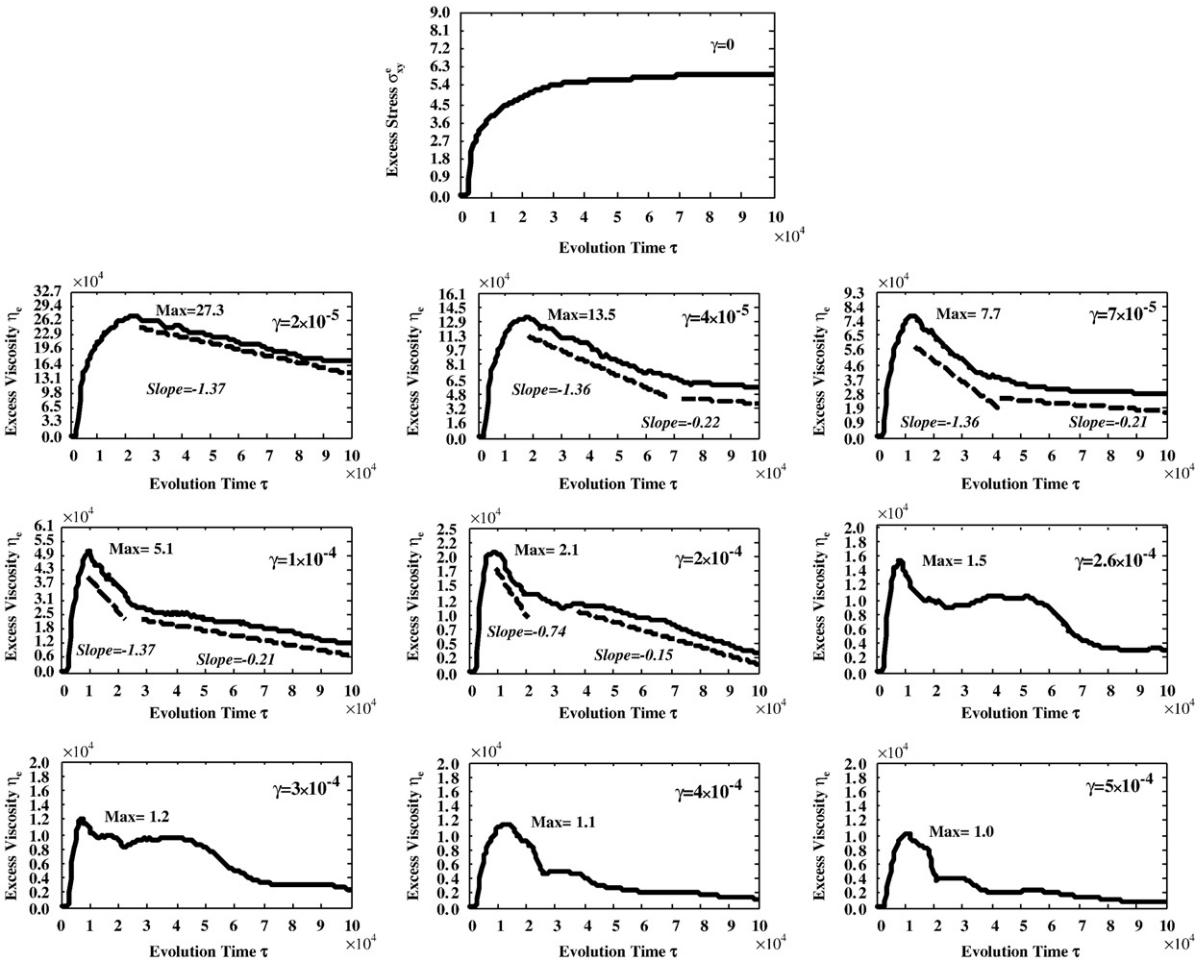

Fig. 6. Plots of time evolution of the excess shear stress σ^e_{xy} for γ=0 and the excess viscosity η_e for different shear rates.

viscosity to increase with time. As the formed string-like domains stretch further, their average orientation gradually leaves the *y* axis and approaches the *x* axis instead. They break up into two or more domains, thus dissipating the stored energy. This is believed to be responsible for the decrease in the excess viscosity. In the strong-shear regime, taking $\gamma=5\times10^{-4}$ for example, in the late stage, the flow acts against the surface tension and induces the stretching of domains, which can also bring about the decrease of η_e. Then due to the utterly elongation along the *x* axis of the domains, η_e eventually vanishes away, as has been confirmed by Hashimoto et al. [49]. The discipline of the decrease process has performed different styles corresponding to the different shear rates. When the shear rate is lower than 1×10^{-4}, this process generally displays two linear steps, with the slope coefficients being independent of the shear rate. But for $\gamma>1\times10^{-4}$, this rule could not stand any more.

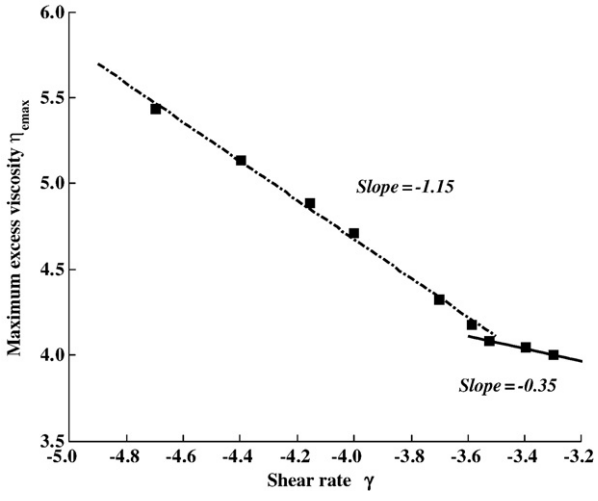

Fig. 7. Log–log plot of the maximum excess viscosity η_{emax} as a function of the shear rate γ.

Finally, we focus on the maximum of η_e, as is labeled in Fig. 6. On the basis of our current results, when $0<\gamma\leq3\times10^{-4}$, the relationship of η_{emax} scaling with the shear rate can be approximately expressed as $\eta_{emax}\sim\gamma^{-1.15}$, whereas for strong-shear regimes it turns to $\eta_{emax}\sim\gamma^{-0.35}$. This is distinctly shown in Fig. 7.

4. Conclusions

In the present paper, we have performed CDS simulations in the two-dimensional space to study domain structures and rheological properties of phase-separating binary lipid membrane undergoing a stationary shear flow. The current results indicate that when shear flow is applied to the system, the time evolution is substantially different from that without such external effect.

Actually, in the early stage of the phase separation, we find that isotropic phase morphologies emerge, indicating that the shear flow has not come into force. Then in the late stage, as the domains go on forming and growing, the anisotropy appears and increases, giving prominence to the effect of the shear flow. At late enough moments, random fluctuating domain patterns are observed in the weak shear

regime, while string-like domains are seen in strong-shear regimes. Subsequently, being the directly gained results of scattering experiments, the dynamical evolution of the structure factor has been simulated as well. Concerning the growth law of the characteristic domain sizes, we found different coarsening behaviors in the two directions parallel and perpendicular to the flow. It is expected that the tendency of minimizing the surface free energy (favoring growth of R_x) and the tendency of breaking up of domains by the flow (suppressing growth of R_y) can balance each other at a steady state so that R_y remains finite. Indicating that the decomposing lipids mixture is endowed with remarkable viscoelastic character, the excess shear stress or the corresponding excess viscosity of the system has been investigated. Our simulations reveal that η_e has an overshoot in the process of domain formation, and the global maximum of η_e behaves as certain distinct functions of the shear rate in weak and strong-shear regimes.

It should be noted that quantitative experiments are absolutely necessary to support the reliability and validity of these numerical simulations. We are in hopes that the present study could give useful insights to the practical control of the phase separation in binary lipid membrane or even in veritable epicyte.

Acknowledgements

The financial support from the Chinese National Natural Science Foundation No. 10672086 and Special Funds for the Major State Basic Research Projects 2004CB619304 are highly appreciated.

Appendix A. Algorithm of numerical implementation

First of all, we easily acquire the integration form of the governing equations in the temporal field

$$\phi(\tau+\Delta\tau)=\phi(\tau)+\Delta\tau \times\left\{-\gamma\cdot\tilde{y}\frac{\partial\phi}{\partial\tilde{x}}+M\nabla^2\left[\left(\tilde{\kappa}\tilde{\Lambda}^2+\tilde{\beta}\right)\phi-\tilde{\alpha}\ \tanh\ (\phi) -\tilde{D}\nabla^2\phi+\tilde{\kappa}\tilde{\Lambda}\nabla^2\tilde{h}\right]\right\} \tag{A1}$$

$$\tilde{h}(\tau+\Delta\tau)=\tilde{h}(\tau)+\Delta\tau\cdot\left\{-\gamma\cdot\tilde{y}\frac{\partial\tilde{h}}{\partial\tilde{x}}-N\left[\tilde{\kappa}\nabla^2\nabla^2\tilde{h}+\tilde{\kappa}\tilde{\Lambda}\nabla^2\phi-\tilde{\lambda}\nabla^2\tilde{h}\right]\right\}. \tag{A2}$$

Then, the Cell Dynamical System (CDS) approach proposed by Puri and Oono [44] is employed to discretize the spatial field. In the CDS model, the two-dimensional system is discretized into a $L\times L$ square lattice (the current computer simulation has been carried out with $L=128$) of the cell size a_0. With this, the order parameter field $\phi(\boldsymbol{n},\tau)$ and the off-plane displacement field $\tilde{h}(\boldsymbol{n},\tau)$ are assigned to each lattice point $\boldsymbol{n}=(n_x,n_y)$ respectively, where we have $n_x,n_y=1,2,3,\ldots,L$. Periodic boundary condition has been imposed in the direction parallel to the flow [44], that means

$$\begin{aligned}\phi(n_x+P(L-1),n_y,\tau)&=\phi(n_x,n_y,\tau)\\ \tilde{h}(n_x+P(L-1),n_y,\tau)&=\tilde{h}(n_x,n_y,\tau).\end{aligned} \tag{A3}$$

But in the direction perpendicular to the flow, there should be some dissimilarities, which can be expressed as [54]

$$\begin{aligned}\phi(n_x+S(\tau)Q(L-1),n_y+Q(L-1),\tau)&=\phi(n_x,n_y,\tau)\\ \tilde{h}(n_x+S(\tau)Q(L-1),n_y+Q(L-1),\tau)&=\tilde{h}(n_x,n_y,\tau)\end{aligned} \tag{A4}$$

where P and Q are arbitrary integers, $S(\tau)=\int_0^\tau\gamma dt=\gamma\tau$ is the temporal strain at the moment τ.

The gradient operator and the Laplacian operator in such two-dimensional square lattice are discretely approximated by [44]

$$\nabla\psi(n_x,n_y)=\frac{1}{2}\left(\psi(n_x+1,n_y)-\psi(n_x-1,n_y),\psi(n_x,n_y+1)-\psi(n_x,n_y-1)\right) \tag{A5}$$

$$\nabla^2\psi=\frac{1}{6}\sum_i\psi_i+\frac{1}{12}\sum_{ii}\psi_{ii}-\psi \tag{A6}$$

where ψ is standing for either ϕ or $\tilde{h}$, i represents nearest-neighbor lattice points and ii represents next-nearest-neighbors.

References

[1] S.L. Veatch, S.L. Keller, Organization in lipid membranes containing cholesterol, Phys. Rev. Lett. 89 (2002) 1–4 268101.
[2] S.J. Singer, G.L. Nicolson, The fluid mosaic model of the structure of cell membranes, Science 175 (1972) 720–731.
[3] T. Kawakatsu, D. Andelman, K. Kawasaki, T. Taniguchi, Phase-transitions and shapes of 2-component membranes and vesicles. 1. Strong segregation limit, J. Phys. II (France) 3 (1993) 971–997.
[4] T. Friedrichson, T.V. Kurzchalia, Microdomains of GPI-anchored proteins in living cells revealed by crosslinking, Nature 394 (1998) 802–805.
[5] W.T. Gozdz, G. Gompper, Shape transformations of two-component membranes under weak tension, Europhys. Lett. 55 (2001) 587–593.
[6] P.B.S. Kumar, G. Gompper, R. Lipowsky, Budding dynamics of multicomponent membranes, Phys. Rev. Lett. 86 (2001) 3911–3914.
[7] K. Simons, E. Ikonen, Functional rafts in cell membranes, Nature 387 (1997) 569–572.
[8] K. Simons, D. Toomre, Lipid rafts and signal transduction, Nat. Rev., Mol. Cell Biol. 1 (2000) 31–39.
[9] T. Harder, P. Scheiele, P. Verkade, K. Simons, Lipid domain structure of the plasma membrane revealed by patching of membrane components, J. Cell Biol. 141 (1998) 929–942.
[10] M. Edidin, Shrinking patches and slippery rafts: scales of domains in the plasma membrane, Trends Cell Biol. 11 (2001) 492–496.
[11] J.R. Silvius, Role of cholesterol in lipid raft formation: lessons from lipid model systems, Biochim. Biophys. Acta, Biomembr. 1610 (2003) 174–183.
[12] S.L. Veatch, S.L. Keller, Separation of liquid phases in giant vesicles of ternary mixtures of phospholipids and cholesterol, Biophys. J. 85 (2003) 3074–3083.
[13] S. Mayor, M. Rao, Rafts: Scale-dependent, active lipid organization at the cell surface,Traffic 5 (2004) 231–240.
[14] S.L. Keller, W.H. Pitcher III, W.H. Huestis, H.M. McConnell, Red blood cell lipids form immiscible liquids, Phys. Rev. Lett. 81 (1998) 5019–5022.
[15] J. Kas, E. Sackmann, Shape transitions and shape stability of giant phospholipids vesicles in pure water induced by area-to-volume changes, Biophys. J. 60 (1991) 825–844.
[16] T. Baumgart, S.T. Hess, W.W. Webb, Imaging coexisting fluid domains in biomembrane models coupling curvature and line tension, Nature 425 (2003) 821–824.
[17] J.C. Lawrence, D.E. Saslowsky, J.M. Edwardson, R.M. Henderson, Realtime analysis of the effects of cholesterol on lipid raft behavior using atomic force microscopy, Biophys. J. 84 (2003) 1827–1832.
[18] C. Nicolini, J. Kraineva, M. Khurana, N. Periasamy, S.S. Funari, R. Winter, Temperature and pressure effects on structural and conformational properties of POPC/SM/cholesterol model raft mixtures—a FT-IR, SAXS, DSC, PPC and Laurdan fluorescence spectroscopy study, Biochim. Biophys. Acta 1758 (2006) 248–258.
[19] N. Kahya, D. Scherfeld, K. Bacia, B. Poolman, P. Schwille, Probing lipid mobility of raft-exhibiting model membranes by fluorescence correlation spectroscopy, J. Biol. Chem. 278 (2003) 28109–28115.
[20] A.D. Albert, K. Boesze-Battaglia, The role of cholesterol in rod outer segment membranes, Prog. Lipid Res. 44 (2005) 99–124.
[21] P.B.S. Kumar, M. Rao, Shape instabilities in the dynamics of a two-component fluid membrane, Phys. Rev. Lett. 80 (1998) 2489–2492.
[22] M. Laradji, P.B.S. Kumar, Dynamics of domain growth in self-assembled fluid vesicles, Phys. Rev. Lett. 93 (2004) 1–4 198105.
[23] E.J. Wallace, N.M. Hooper, P.D. Olmsted, The kinetics of phase separation in asymmetric membranes, Biophys. J. 88 (2005) 4072–4083.
[24] H. Wada, Dynamics of phase separation in confined two-component fluid membranes, J. Phys. Soc. Jpn. 72 (12) (2004) 3142–3150.
[25] R. Reigada, J. Buceta, K. Lindenberg, Nonequilibrium patterns and shape fluctuations in reactive membranes, Phys. Rev., E 71 (2005) 051906.
[26] T. Nakajima, K. Kon, N. Maeda, K. Tsunekawa, T. Shiga, Deformation response of red blood cells in oscillatory shear flow, Am. J. Physiol., Heart Circ. Physiol. 259 (1990) H1071–H1078.
[27] C.H. Wang, A.S. Popel, Effect of red blood cell shape on oxygen transport in capillaries, Math. Biosci. 116 (1993) 89–110.
[28] S. Chien, S. Usami, R.J. Dellenback, M.I. Gregersen, Shear-dependent deformation of erythrocytes in rheology of human blood, Am. J. Physiol. 219 (1970) 136–143.
[29] M.A. Haidekker, N. L'Heureux, J.A. Frangos, Fluid shear stress increases membrane fluidity in endothelial cells: a study with DCVJ fluorescence, Am. J. Physiol., Heart Circ. Physiol. 278 (2000) H1401–H1406.

[30] P.J. Butler, G. Norwich, S. Weinbaum, S. Chien, Shear stress induces a time- and position-dependent increase in endothelial cell membrane fluidity, Am. J. Physiol. Cell Physiol. 280 (2001) C962–C969.
[31] A.J. Bray, K. Humayun, Scaling and multiscaling in the ordering kinetics of a conserved order parameter, Phys. Rev. Lett. 68 (1992) 1559–1562.
[32] D. Orlikowski, C. Sagui, A. Somaza, C. Roland, Large-scale simulation of phase separation of elastically coherent binary alloy systems, Phys. Rev., B 59 (1999) 8646–8659.
[33] J.-I. Fukuda, Phase separation kinetics of liquid crystalline polymers: Effect of orientational order, Phys. Rev., E 59 (1999) 3275–3288.
[34] J.W. Cahn, J.E. Hilliard, Free energy of a nonuniform system. I. Interfacial free energy, J. Chem. Phys. 28 (1958) 258–267.
[35] J.W. Cahn, Free energy of a nonuniform system. II. Thermodynamic basis, J. Chem. Phys. 30 (1959) 1121–1124.
[36] J.W. Cahn, J.E. Hilliard, Free energy of a nonuniform system. III. Nucleation in a two-component incompressible fluid, J. Chem. Phys. 31 (1959) 688–699.
[37] K.-T. Leung, Theory on morphological instability in driven systems, J. Stat. Phys. 61 (1990) 345–364.
[38] D.H. Rothman, Deformation, growth, and order in sheared spinodal decomposition, Phys. Rev. Lett. 65 (1990) 3305–3308.
[39] C. Yeung, T. Rogers, A. Hernandez-Machado, D. Jasnow, Phase separation dynamics in driven diffusive systems, J. Stat. Phys. 66 (1992) 1071–1088.
[40] C.L. Emmott, A.J. Bray, Coarsening dynamics of a one-dimensional driven Cahn–Hilliard system, Phys. Rev., E 54 (1996) 4568–4575.
[41] R. Yamamoto, X.C. Zeng, Molecular dynamics study of a phase-separating fluid mixture under shear flow, Phys. Rev., E 59 (1999) 3223–3230.
[42] A.H. Krall, J.V. Sengers, K. Hamano, Experimental studies of the rheology of a simple liquid mixture during phase separation, Phys. Rev., E 48 (1993) 357–376.
[43] A.A. Golovin, A.A. Nepomnyashchy, S.H. Davis, M.A. Zaks, Convective Cahn–Hilliard models: From coarsening to roughening, Phys. Rev. Lett. 86 (2001) 1550–1553.
[44] Y. Oono, S. Puri, Study of phase-separation dynamics by use of cell dynamical systems. I. Modeling, Phys. Rev., A 38 (1988) 434–453.
[45] U. Seifert, Configurations of fluid membranes and vesicles, Adv. Phys. 46 (1997) 13–137.
[46] T. Ohta, Y. Enomoto, Anomalous rheological behavior of ordered phases of block copolymers. 1, Macromolecules 26 (1993) 4928–4934.
[47] S. Ramaswamy, Shear-induced collapse of the dilute lamellar phase, Phys. Rev. Lett. 69 (1992) 112–115.
[48] H. Kodama, M. Doi, Shear-induced instability of the lamellar phase of a block copolymer, Macromolecules 29 (1996) 2652–2658.
[49] T. Hashimoto, K. Matsuzaka, E. Moses, A. Onuki, String phase in phase-separating fluid under shear flow, Phys. Rev. Lett. 74 (1995) 126–129.
[50] R.E. Waugh, Surface viscosity measurements from large bilayer vesicle tether formation: II. Experiments, Biophys. J. 38 (1982) 29–37.
[51] G. Maksimov, O. Luneva, N. Maksimova, E. Matettuchi, E. Medvedev, V. Pashchenko, A. Rubin, Role of viscosity and permeability of the erythrocyte plasma membrane in changes in oxygen-binding properties of hemoglobin during diabetes mellitus, B. Exp. Biol. Med. 140 (5) (2005) 510–513.
[52] A. Onuki, Viscosity enhancement by domains in phase-separating fluids near the critical point: Proposal of critical rheology, Phys. Rev., A 35 (1987) 5149–5155.
[53] H. Miyazawa, H. Tanaka, Nucleation of lamellar domains from a sponge phase under shear flow: Shape selection of nuclei in a nonequilibrium steady state, Phys. Rev., E 76 (2007) 1–9 011513.
[54] A. Onuki, A new computer method of solving dynamic equations under externally applied deformation, J. Phys. Soc. Jpn. 66 (6) (1997) 1836–1837.